Analytical and Bioanalytical Chemistry
https://doi.org/10.1007/s00216-019-01776-4

RESEARCH PAPER

Rapid and noninvasive diagnostics of Huanglongbing and nutrient deficits on citrus trees with a handheld Raman spectrometer

Lee Sanchez[1] · Shankar Pant[2] · Zhongliang Xing[1] · Kranthi Mandadi[2,3] · Dmitry Kurouski[1,4]

Received: 11 February 2019 / Accepted: 11 March 2019

Abstract

Huanglongbing (HLB) or citrus greening is a devastating disease of citrus trees that is caused by the gram-negative *Candidatus* Liberibacter spp. bacteria. The bacteria are phloem limited and transmitted by the Asian citrus psyllid, *Diaphorina citri*, and the African citrus psyllid, *Trioza erytreae*, which allows for a wider dissemination of HLB. Infected trees exhibit yellowing of leaves, premature leaf and fruit drop, and ultimately the death of the entire plant. Polymerase chain reaction (PCR) and antibody-based assays (ELISA and/or immunoblot) are commonly used methods for HLB diagnostics. However, they are costly, time-consuming, and destructive to the sample and often not sensitive enough to detect the pathogen very early in the infection stage. Raman spectroscopy (RS) is a noninvasive, nondestructive, analytical technique which provides insight into the chemical structures of a specimen. In this study, by using a handheld Raman system in combination with chemometric analyses, we can readily distinguish between healthy and HLB (early and late stage)-infected citrus trees, as well as plants suffering from nutrient deficits. The detection rate of Raman-based diagnostics of healthy vs HLB infected vs nutrient deficit is ~ 98% for grapefruit and ~ 87% for orange trees, whereas the accuracy of early- vs late-stage HLB infected is 100% for grapefruits and ~94% for oranges. This analysis is portable and sample agnostic, suggesting that it could be utilized for other crops and conducted autonomously.

Keywords Raman spectroscopy · Plant diseases · Huanglongbing · Chemometrics · Nutrient deficiency

Introduction

Global food security is one of the most important aspects of our civilization and its importance will only increase in the future. Currently, over a billion people suffer from a lack of sufficient nutrition, whereas by 2050, we will need 70% more food [1]. This problem can be potentially solved by an expansion of agricultural land areas. However, this approach is resource intensive and unsustainable to the environment. The second strategy is to develop methodology for timely detection and identification of plant diseases. This will allow for a selective pathogen treatment in a certain area of the field. Such a precise disease treatment is economically advantageous and has a potential of saving up to 50% of the total agricultural yield worldwide [2].

Huanglongbing (HLB), otherwise known as citrus greening, is a psyllid-vectored bacterial disease [3, 4] that plagues the largest citrus-producing regions in the world: Asia, Africa, and more recently the Americas [5]. The pathogen associated with this disease is a fastidious (unculturable) bacterium [6], *Candidatus* Liberibacter spp. (CLas), which inhabits in the plant phloem tissues. Furthermore, the bacterium is slow growing and is present in variable titers in the plant tissues [7]. In later stages of the disease, characteristic symptoms of asymmetric mottling on the leaves, lopsided and green fruits, and overall stunting of the trees occur. Early stages of the disease, however, have minimal to no symptoms and the bacteria can remain undetectable even by polymerase chain reaction (PCR) in the trees for several years after initial infection [8]. This, wherein, lies a significant challenge in detecting the pathogen leading to poor HLB management. Growers are

Electronic supplementary material The online version of this article (https://doi.org/10.1007/s00216-019-01776-4) contains supplementary material, which is available to authorized users.

✉ Dmitry Kurouski
dkurouski@tamu.edu

[1] Department of Biochemistry and Biophysics, Texas A&M University, College Station, TX 77843, USA

[2] Texas A&M AgriLife Research and Extension Center at Weslaco, Weslaco, TX 78596, USA

[3] Department of Plant Pathology and Microbiology, Texas A&M University, College Station, TX 77843, USA

[4] The Institute for Quantum Science and Engineering, Texas A&M University, College Station, TX 77843, USA

Published online: 15 April 2019

reluctant to remove trees that appear healthy and yield normal, yet the trees could be latent reservoirs for inoculum, allowing psyllids to spread the disease. It is very critical to detect HLB at the early or pre-symptomatic stage to deploy appropriate intervention strategies for further containment of HLB.

Several diagnostic methods, such as PCR and enzyme-linked immunosorbent assay (ELISA), are commonly used for the confirmatory diagnostics of plant diseases, including HLB. However, these molecular methods have their own limitations. ELISA, for instance, including double- and triple-antibody ELISA, has low sensitivity, photobleaching instability, and poor specificity related to pathogen strains [9, 10]. PCR-based and quantitative real-time PCR (qPCR)–based techniques have been successfully used for detection and quantification of the HLB in citrus [11, 12]. However, PCR has limited portability and is labor intensive and costly. There is also a need of specific expertise and it is destructive to the analyzed specimen [13–15]. Moreover, certain minimal amount of bacterial titer is required for accurate detection of pathogen with PCR-based method [12]. As a result, these limitations catalyzed a push toward developing sensitive and minimally invasive techniques that can be used directly in the field for reliable and early detection of HLB, which will allow deploying intervention strategies before the disease spreads further.

Raman spectroscopy (RS) is a label-free, noninvasive, nondestructive spectroscopic technique that provides information about the chemical structure of analyzed specimens. RS is commonly used in food chemistry [16], electrochemistry [17], forensics [18, 19], and materials science [20]. It is capable of monitoring changes in protein secondary structure [21] and elucidating composition and origin of body fluids [18] as well as gunshot residues [22]. While RS is generally known to be a technique used in-lab, the past decade has seen several developments of portable Raman spectrometers, which has enabled the utilization of RS directly in the field.

At the fundamental level, unlike conventional diagnostics that detect mainly the pathogen titers, the RS diagnostics approach is based on a detection of a consortium of pathogen-induced changes in host molecules, which are highly specific to an individual disease or condition. These structural changes are reflected in shifts or changes in intensities of specific Raman bands that can be assigned to those molecules. This makes RS both useful and sensitive in capturing the signatures of early infection when the pathogen is at a very low level for detection. Additionally, RS is noninvasive and nondestructive. Our group has recently demonstrated that using a handheld Raman system, we can detect and identify common fungal diseases caused by culturable pathogens of maize, wheat, and sorghum [23, 24]. For instance, we were able to identify whether maize kernels were healthy or infected by *Aspergillus flavus*, *A. niger*, *Fusarium* spp., or *Diplodia* spp. with 100% accuracy. We also showed that RS could be used for identification of both single or multi-pathogen-induced plant diseases such as ergot and mold, respectively. In addition to fungal disease diagnostics, we have recently shown that RS can be used to detect insect larva within beans, detecting not only their presence but also, using statistical models, their developmental stage [25]. In this study, we have demonstrated that RS could be used to detect HLB on early and late stages of disease development. We also show that RS can be used to distinct between nutrient deficiency and HLB disease.

Materials and methods

Plants

Orange (*Citrus sinensis*, Valencia) and grapefruit (*Citrus paradasi*, Rio red) field samples were collected from RioFarms, Monte Alto, TX (26° 22′ 22.1″ N, 97° 59′ 03.3″ W) and Texas A&M University-Kingsville Citrus Center, Weslaco, TX (26° 10′ 00.1″ N, 97° 57′ 27.7″ W). Twelve to 21 leaves were collected randomly from each healthy, nutrient-deficient (ND), and HLB early-stage (non-symptomatic) and late-stage (symptomatic) tree (Fig. 1). Precautions were taken to collect leaves devoid of any physical or insect damage, as well as symptoms unrelated to HLB. Such leaves with no direct relationship to HLB could complicate interpretation with the overlapping spectral data. Therefore, such leaves were excluded from sampling. Also, samples were analyzed in two independent experiments, about 2 months apart from each other. This was done to eliminate any possible environmental factors/bias. All samples were transferred to Ziploc bags and immediately brought to lab for Raman spectroscopy and qPCR analysis.

Raman spectroscopy

Following collection of the citrus leaves in-field, Raman spectra were taken with a handheld Resolve Agilent spectrometer equipped with 831-nm laser source (beam diameter ~ 2 mm). The following experimental parameters were used for all collected spectra: 1-s acquisition time, 495-mW power, and baseline spectral subtraction by device software. Visual examination of the analyzed leaf areas after spectral acquisition showed no signs of photodegradation or thermal degradation of plant tissue (see Electronic Supplementary Material (ESM) Fig. S1). Four spectra were collected from each leaf from four quadrants on the adaxial side of the leaf. In total, around 50 surface spectra from each group (healthy, HLB late and early stage, as well as ND) were collected. Averaged

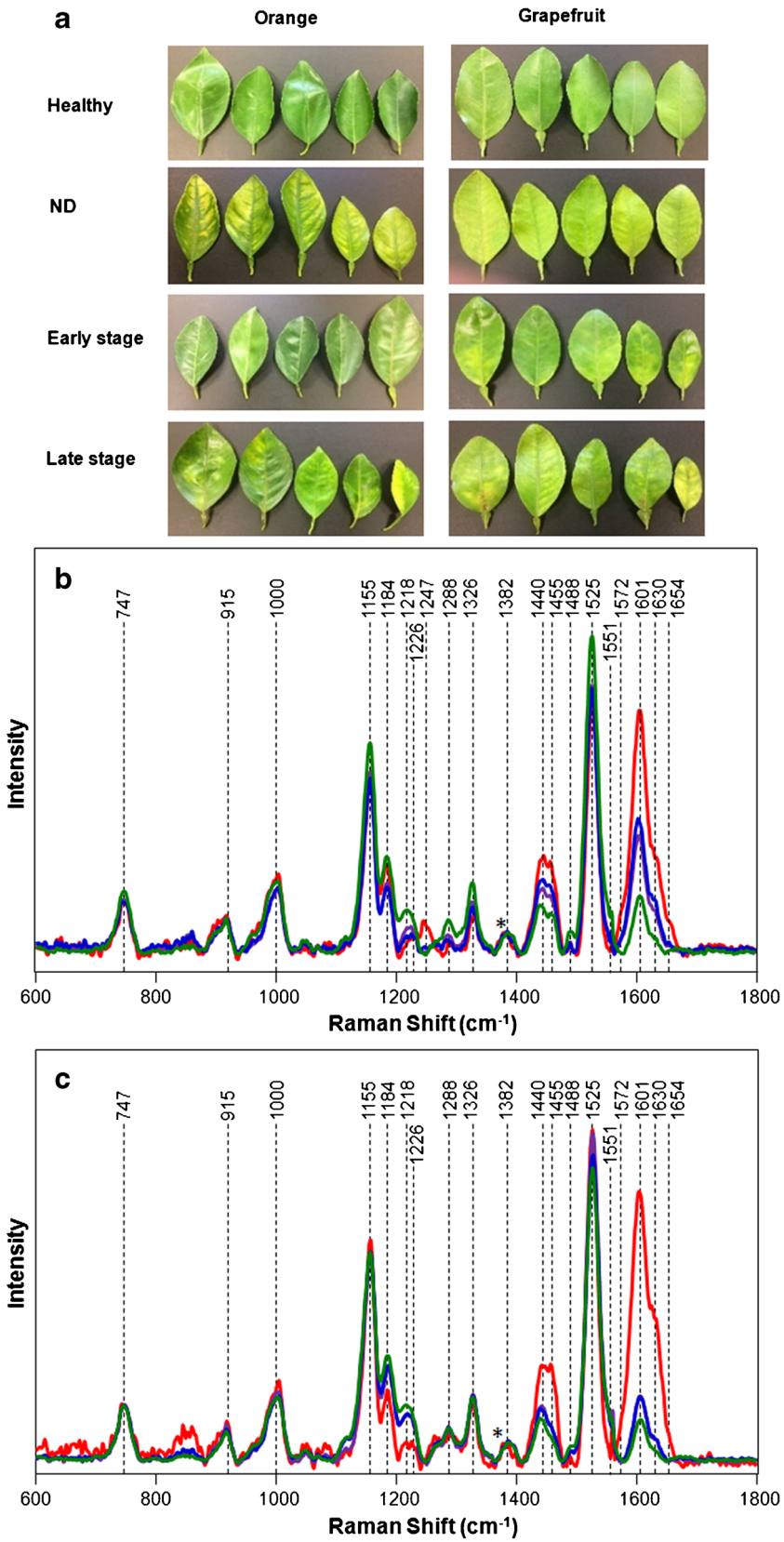

Fig. 1 Leaf samples collected from fields for qPCR assay and Raman spectrum (**a**). Raman spectra generated from leaves of healthy (green), HLB infected on late (blue) and early (purple) stages, and nutrient-deficit (ND) symptoms (red) grapefruit (**b**) and orange (**c**) trees. Spectra normalized on CH_2 vibration that is present in nearly all classes in biological molecules (marked by asterisks (*))

spectra for each group of plants along with their standard deviations are shown in the ESM (Figs. S2 and S3). Spectra shown in the manuscript are raw baseline corrected, without smoothing.

DNA extraction

After taking Raman spectra readings, DNA was extracted from each leaf, according to [26, 27] with minor modifications as follows: ~ 200 mg of finely sliced leaf tissue was homogenized in 2-ml screw cap microcentrifuge tubes for 45 s at 5000 rpm with the Precellys 24 homogenizer (MO BIO Laboratories, Carlsbad, CA, USA) in the presence of two steel BB air gun beads (BB refers to the bead size, 4.5-mm diameter) (Walmart Supercenter, Bentonville, AR, USA). DNA was quantified by measuring the concentration using a NanoDrop 1000 Spectrophotometer (Thermo Fisher Scientific, Wilmington, DE, USA). The quality of DNA was examined by electrophoresis on 1% agarose gels stained with ethidium bromide.

Quantitative real-time PCR

Quantitative real-time PCR (qPCR) was performed to determine presence/absence of HLB in healthy, nutrient-deficient, and HLB early- and late-stage leaf DNA. Forward primer rplk04 (5′-GGATAGTCCTGTTATTGCTCCTAAA-3′) and reverse primer J5 (5′-ACAAAAGCAGAAATAGCACG AACAA-3′) combination was used to amplify the *ribosomal protein* gene in the CLas [11]. The citrus endogenous gene glyceraldehyde-3-phosphate dehydrogenase C2 (GAPC2) [28] was used as internal control and for normalization of qPCR data. The qPCR assays were performed using a CFX384™ Real-Time PCR Detection System (Bio-Rad Laboratories, Inc., Hercules, CA, USA) with the iTaq™ universal SYBR® Green supermix (Bio-Rad Laboratories, Inc.), 0.2 μM of target specific primer, and 50 ng of genomic DNA, according to the manufacturer's instructions. qPCR was performed with two technical replicates per sample using the following conditions: 1 cycle at 95 °C for 3 min, 39 two-step cycles each at 95 °C for 15 s and 57 °C for 30 s, and a final melting curve of 65–95 °C for 5 s. Results were analyzed and recorded as threshold cycle (Ct) values after normalization with the citrus housekeeping gene GAPC2. Post-amplification dissociation curve was performed and only a single amplicon peak was detected suggesting no non-specific amplification. For this study, samples with a Ct value of ≤ 28 were considered as HLB positive.

Multivariate data analysis

SIMCA 14 (Umetrics, Umeå, Sweden) was used for statistical analysis of the collected Raman spectra. All imported spectra were scaled to unit variance to give all spectral regions equal importance. Orthogonal partial least squares discriminant analysis (OPLS-DA) was performed in order to determine the number of significant components and identify spectral regions that best explain the separation between the classes. In order to give each of the spectral regions equal importance, all spectra were scaled to unit variance. Raw spectra, containing wavenumbers 350–2000 cm^{-1}, were retained in the model that resulted from this iteration of OPLS-DA.

Results and discussion

We used a handheld Raman spectrometer with 831-nm excitation to investigate healthy and HLB-infected orange and grapefruit trees, as well as trees suffering from ND whose symptoms were similar to HLB symptomatology. This spectrometer allows for collection of excellent signal-to-noise spectra in only 1-s acquisition time, which makes the Raman-based pathogen diagnostics suitable for rapid and high-throughput detection and identification of plant diseases. Additionally, the same leaves used for Raman-based studies were analyzed and compared with conventional molecular diagnostic tools (qPCR). Raman spectrum of healthy citrus leaves exhibited vibrational bands originating from cellulose, lignin, pectin, proteins, and carotenoids (Fig. 1, Table 1). We also observed CH_2 and CH_3 vibrational bands that can be assigned to aliphatic hydrocarbons, such as oils and waxes.

Lignin plays a key role in plant defense, as well as abiotic and physiological stresses [42]. We observed a significant increase in the intensity of 1601–1630 cm^{-1} bands that could be assigned to lignin. Moreover, intensities of these bands in Raman spectra collected from grapefruit leaves with late-stage HLB infection are higher compared with the spectra of early-stage HLB-infected leaves. The intensities of these bands in Raman spectra collected from orange leaves with late- and early-stage HLB were nearly identical. The increase in the intensities of these bands is even more pronounced in the spectra of both grapefruit and orange leaves that have ND symptoms. Thus, one can envision that ND may have a unique vibrational fingerprint related to lignin that is distinctly higher from Raman signatures of both healthy and HLB-infected leaves.

We observed significant changes in the intensities of 1440–1455 cm^{-1} bands (CH_2 and CH_3 vibrations) in the Raman spectra collected from both grapefruit and orange leaves. We also found that both grapefruit and orange leaves with ND exhibited higher intensities of these bands compared with both healthy and HLB-infected leaves. Interestingly, grapefruit ND exhibited a band at 1247 cm^{-1} which could be assigned to phenolic compounds, whereas this band was not evident in the spectrum of orange leaves that were phenotypically similar to ND. Since ND could be caused by a lack of various nutrients and the physiological response of the plant could be different in each specific case of ND, these findings suggest that RS could be used to disentangle specific NDs in plants. Further work is required for experimental validation of this hypothesis. Nevertheless, the ability of using RS to

Table 1 Vibrational bands and their assignments for healthy, HLB, and nutrient-deficit leaves from orange and grapefruit trees

Band	Vibrational mode	Assignment
747	γ(C–O–H) of COOH	Pectin [29]
915	ν(C–O–C) in plane, symmetric	Cellulose, lignin [30]
1000	ν_3 (C–CH_3 stretching) and phenylalanine	Carotenoids [31, 32]
1155	asym ν(C–C) ring breathing	Cellulose [30]
1184	ν(C–O–H) next to aromatic ring+σ(CH)	Xylan [33, 34]
1218–1226	δ(C–C–H)	Aliphatic [35], xylan [33]
1247	C–O stretching (aromatic)	Phenolic [36]
1288	δ(C–C–H)	Aliphatic [35]
1326	δCH_2 bending vibration	Cellulose, lignin [30]
1382	δCH_2 bending vibration	Aliphatic [35]
1440	δ(CH_2)+δ(CH_3)	Aliphatic [35]
1455	δCH_2 bending vibration	Aliphatic [35]
1488	δ(CH_2)+δ(CH_3)	Aliphatic [35]
1527–1551	–C=C– (in plane)	Carotenoids [37, 38]
1601	ν(C–C) aromatic ring+σ(CH)	Lignin [39, 40]
1630	C=C–C (ring)	Lignin [39–41]
1654	C=O stretching, amide I	Proteins (α-helix) [37]

differentiate ND from HLB-infected tissues is significant since nutrient and HLB symptoms have often overlapping symptoms.

Both orange and grapefruit leaves of HLB-infected trees exhibited similar changes in the 1184–1230 cm^{-1} spectral region. The intensities of 1184, 1218, and 1226 cm^{-1} bands in the Raman spectra collected from HLB-infected leaves are lower compared with intensities of the corresponding bands in the Raman spectra of healthy leaves. These vibrational bands could be assigned to xylan and similar carbohydrates. This indicates that HLB infection is associated with changes in carbohydrate content of citrus leaves. Additionally, in the Raman spectrum of healthy grapefruit leaves, 1218 cm^{-1} band has higher intensity compared with 1226 cm^{-1} band, whereas the ratio is opposite in HLB-infected grapefruit leaves. Interestingly, those ratios of these bands remained the same in the spectra collected from healthy and HLB-infected orange leaves.

We also found that the intensity of 1184 cm^{-1} band is higher in the spectra collected from grapefruit leave with ND symptoms compared with Raman spectra collected from healthy and HLB-infected leaves. At the same time, this band, as well as 1218–1226 cm^{-1} bands, has lower intensities in the spectra collected from ND orange leaves relative to the healthy and HLB-infected leaves of orange trees. These findings indicate that ND also affects structure and composition of xylan and similar carbohydrates in both oranges and grapefruits. Moreover, these changes appear to be either plant or ND specific. Additional studies are required to disentangle these two possibilities for the origin of the observed spectral changes.

Biotic stress can trigger secondary defense metabolites such as carotenoids and flavonoids [43–45]. In the spectra of HLB-infected grapefruit leaves, we observed no significant changes in the intensity or position of the vibrational band which could be assigned to carotenoids (~ 1525 cm^{-1}). This indicates that HLB is not associated with a change in the structure and/or composition of carotenoids in the leaves of grapefruits. However, we observed a small increase in the intensity of carotenoids in the spectra of HLB, as well as ND symptomatic orange leaves. This suggests that HLB infection as well as ND deficits is associated with small changes in carotenoids in oranges, but not in grapefruits. It is very likely that orange and grapefruit plants have cultivar-specific responses to various stresses.

We also observed significant changes in intensities of 1654 cm^{-1} band, which could be assigned to macromolecules such as proteins. Intensity and position of this band did not change in HLB-infected orange and grapefruit leaves, whereas significant increase in its intensity was observed in the spectra collected from both orange and grapefruit leaves with ND symptoms. This suggests that ND is associated with the change in protein content in both orange and grapefruit trees.

Next, we applied multivariate data analysis [47] to determine whether RS could be used for highly accurate diagnostics of HLB and ND on grapefruit and orange leaves [48]. The loading plot (Fig. 2) and misclassification table (Tables 2, 3, 4, and 5) were then generated using this final model, which contained 3 predictive components, 4 orthogonal components, and 1651 original wavenumbers. Predictive components (PC) 1, 2, and 3 (Fig. 2) explained 30%, 20%, and 17% of variation between the different classes, respectively. Absolute intensities in the loadings spectra were proportional to the percentage of

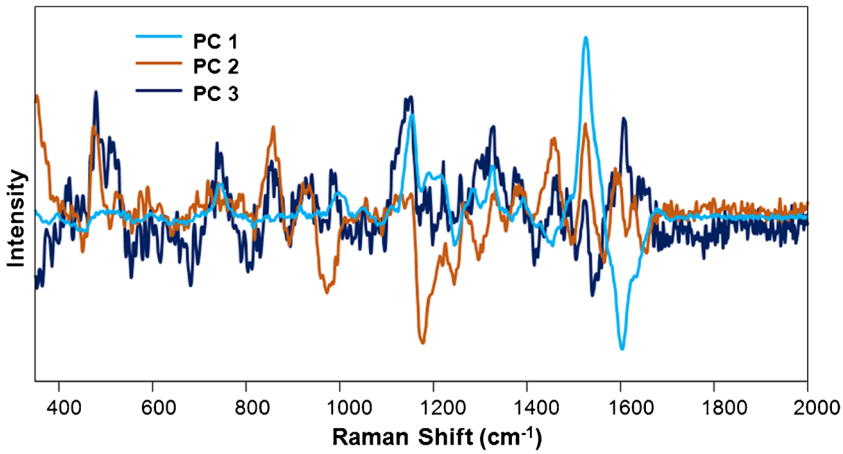

Fig. 2 Loading plot of the three predictive components (PC) in the Raman spectra of citrus leaves

the total variation between classes explained by each wavenumber within each component. The model identified the carotenoids peak at 1528 cm^{-1} (PC1), lignin peaks at 1604 cm^{-1} (PC1), cellulose peaks at 1155 cm^{-1} (PC1), the xylan band at 1180 cm^{-1} (PC2), the hydrocarbon bond vibration at 1455 cm^{-1} (PC2), and the cellulose and lignin peak at 1329 cm^{-1} (PC3) as the strongest predictors of the pathogens, which supports the conclusions of our qualitative spectral analysis presented above. The model also explained 76% of the variation (R2X) in the spectra and 67% (R2Y) of the variation between the classes. Furthermore, the model correctly assigned over 85% of the spectra to their classes (Tables 2, 3, 4, and 5). This indicates that coupling of OPLS-DA with RS allows for a high-accuracy detection and identification of these four classes. These results are very encouraging and demonstrated that RS can be a reliable tool to detect HLB in citrus leaves with high accuracy and differentiate healthy, HLB, and ND samples.

To compare the RS results with conventional approaches, we performed qPCR diagnostics to detect CLas pathogen, using the same leaf samples that were used for Raman spectral reading (Fig. 1a). The qPCR results are presented as Ct values after normalization with a citrus housekeeping gene GAPC2 (Fig. 3). A cutoff value ($Ct \leq 28$) was used to categorize the sample as HLB positive. Among the ND samples, except for one sample in orange (Fig. 3b), all of them were HLB negative. Among late-stage HLB-infected orange and grapefruit samples, 100% and 91.6% of the samples were positive by qPCR, respectively. RS predictions were 100% and 86% for orange and grapefruit samples, respectively. These results demonstrate that the RS method is highly congruent with qPCR for HLB diagnostics.

It is widely known among the HLB research community that the titers of CLas are often undetectable in early stages of infection, which could span several months to years before onset of symptoms and being detectable by qPCR. Furthermore, the bacterial titers are variable within an infected plant or a branch. Among the early-stage orange samples, 50% of the samples were found to be HLB positive based on qPCR. In contrast, RS predicted 83.3% as HLB positive. One explanation for the lower detection rate in qPCR assay may be attributed partly to the detection limits of qPCR for CLas in early stage of disease. Among the early-stage grapefruit samples, 83.3% were found to be HLB positive based on qPCR, which is comparable with the RS prediction (85%). The differences in qPCR detection rate among the early grapefruit and orange samples could be a result of the age of the trees. The grapefruit orchard we sampled had more HLB-positive trees than the orange. We also know that this orchard was infected by HLB for a longer period, thus may have allowed for CLas titers to accumulate in the trees. Nevertheless, together, these results demonstrate that RS method is comparable, if not more sensitive, than qPCR in HLB detection and early-stage diagnosis.

Advanced HLB diagnostics has been the active research topic during the last decades. For instance, Sankaran and co-

Table 2 Accuracy of classification by OPLS-DA for healthy, HLB-infected, and ND classes of grapefruit leaves

	Members	Correct	Healthy	Nutrient	HLB infected
Healthy	60	100%	60	0	0
Nutrient	52	100%	0	52	0
HLB infected	83	95.2%	1	3	79
Total	195	98.0%	61	55	79
Fisher's prob.	4.7e−025				

Table 3 Accuracy of classification by OPLS-DA for early- and late-stage HLB-infected grapefruit leaves

	Members	Correct	Early-stage HLB	Late-stage HLB
Early-stage HLB	40	100.0%	40	0
Late-stage HLB	43	100.0%	0	43
Total	83	100.0%	40	43
Fisher's prob.	3e−006			

Table 4 Accuracy of classification by OPLS-DA for healthy, HLB-infected, and ND classes of orange leaves

	Members	Correct	Healthy	Nutrient	HLB infected
Healthy	84	97.6%	82	0	2
Nutrient	51	94.1%	1	48	2
HLB infected	72	69.4%	22	0	50
Total	207	87.0%	105	48	54
Fisher's prob.	1.6e−006				

workers proposed to use Vis near-IR reflectance to detect HLB on citrus trees [49]. In combination with multivariate statistical analysis, the researchers were able to achieve high accuracy of the disease diagnostics. However, such diagnostics is based on the color difference between leaves of healthy and diseased trees and, therefore, cannot be conclusive because change in leaf color can be associated with drought or nutrient stresses. Infrared spectroscopy (IR) offers a unique opportunity to probe structural changes in plants that are associated with plant diseases. Sankaran and co-workers used mid-IR to detect HLB and nutrient deficits on citrus trees. The researchers achieved nearly 90% accuracy of prediction based on the collected spectra [46]. Similar results have been independently reported by Hawkins and coworkers [50]. It should be noted that plant material had to be dried and grinded prior to IR analysis. These destructive procedures were necessary to remove or minimize the contribution of water which significantly contributes to the collected IR signals. The first actual noninvasive and nondestructive diagnostics of HLB was recently reported by Vallejo-Pérez and co-workers [51]. Using Raman spectroscopy, the researchers observed changes in the background of Raman spectra collected from HLB-positive and healthy leaves of orange trees. However, the spectral background of HLB-positive samples was not differentiated from HLB-negative citrus plants going through ND. Thus, these background-based spectral changes are not reliable and specific for the selective HLB detection. At the same time, our work revealed that both HLB and ND have specific vibrational fingerprint in the Raman spectra of citrus leaves. These spectral differences enable highly accurate detection and identification of HLB and ND.

Table 5 Accuracy of classification by OPLS-DA for early- and late-stage HLB-infected orange leaves

	Members	Correct	Early-stage HLB	Late-stage HLB
Early-stage HLB	24	83.3%	20	4
Late-stage HLB	48	100.0%	0	48
Total	72	94.4%	20	52
Fisher's prob.	3e−006			

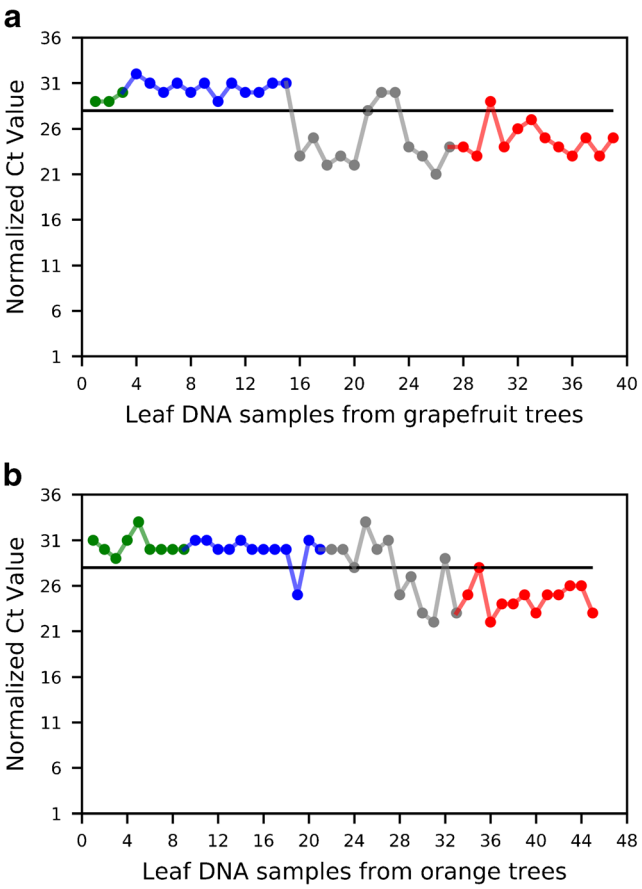

Fig. 3 Quantitative real-time PCR (qPCR)–based diagnostics of healthy (green), ND (blue), and early-stage (gray) and late-stage (red) leaf DNA samples from grapefruit (**a**) and orange (**b**) trees for HLB positive or negative. Solid black line is the normalized Ct cutoff value (Ct ≤ 28) for HLB-positive (below) samples

Conclusions

Our detailed analysis here of healthy, HLB-infected, and ND citrus shows that RS can be reliably used for accurate diagnostics of the unculturable pathogen that causes HLB in citrus trees. A key advantage of RS is the ability to offer greater sensitivity in diagnosing HLB, which is based on unique chemical signatures of the infected cells in early stage when the CLas titers are well below the detection limits of qPCR. In conclusion, we suggest that RS is a rapid and noninvasive diagnostics tool that is portable for in-field applications and allows for early and accurate HLB diagnostics, thus helping in timely intervention and management of these challenging pathogens.

Acknowledgements The authors thank Texas A&M University-Kingsville, Citrus Center, and Riofarms, TX, for access to the citrus orchards.

Funding information This study was supported by funds from Texas A&M AgriLife Research, Texas A&M University Governor's University Research Initiative (GURI) grant program (12-2016/M1700437) to DK, and USDA-NIFA-AFRI (2018-70016-28198) to KKM.

Compliance with ethical standards

Conflict of interest The authors declare that they have no competing interests.

References

1. How to Feed the World 2050. In: Food and Agriculture Organization of the United Nations. 2009. http://www.fao.org/fileadmin/templates/wsfs/docs/expert_paper/How_to_Feed_the_World_in_2050.pdf. Accessed 11 Feb 2019.
2. Savary S, Ficke A, Aubertot J-N, Hollier C. Crop losses due to diseases and their implications for global food production losses and food security. Food Secur. 2012;4:519–37.
3. McClean APD, Oberholzer PCJ. Citrus psylla, a vector of the greening disease of sweet orange. S Afr J Agric Sci. 1965;8:297–8.
4. Capoor SP, Rao DG, Viswanath SM. Diaphorina citri Kuway., a vector of the greening disease of citrus in India. Ind J Agric Sci. 1967;37:572–6.
5. Bové JM. Huanglongbing: a destructive, newly-emerging, century-old disease of citrus. J Plant Pathol. 2006;88:7–37.
6. Tsai JH, Liu YH. Biology of Diaphorina citri (Homoptera: Psyllidae) on four host plants. J Econ Entomol. 2000;93:1721–5.
7. Morgan JK, Zhou L, Li W, Shatters RG, Keremane M, Duan YP. Improved real-time PCR detection of 'Candidatus Liberibacter asiaticus' from citrus and psyllid hosts by targeting the intragenic tandem-repeats of its prophage genes. Mol Cell Probes. 2012;26:90–8.
8. Lee JA, Halbert SE, Dawson WO, Robertson CJ, Keesling JE, Singer BH. Asymptomatic spread of huanglongbing and implications for disease control. Proc Natl Acad Sci U S A. 2015;112:7605–10.
9. Chitarra LG, Bulk RW. The application of flow cytometry and fluorescent probe technology for detection and assessment of viability of plant pathogenic bacteria. Eur J Plant Pathol. 2003;109:407–17.
10. Wallner G, Amann R, Beisker W. Optimizing fluorescent in situ hybridization with rRNA-targeted oligonucleotide probes for flow cytometric identification of microorganisms. Cytometry. 1993;14:136–43.
11. Hocquellet A, Toorawa P, Bove JM, Garnier M. Detection and identification of the two Candidatus Liberobacter species associated with citrus huanglongbing by PCR amplification of ribosomal protein genes of the beta operon. Mol Cell Probes. 1999;13:373–9.
12. Kim J, Wang N. Characterization of copy numbers of 16S rDNA and 16S rRNA of Candidatus Liberibacter asiaticus and the implication in detection in planta using quantitative PCR. BMC Res Notes. 2009;2:37.
13. Schaad NW, Frederick RD. Real-time PCR and its application for rapid plant disease diagnostics. Can J Plant Pathol. 2002;24:250–8.
14. Wang Z, Yin Y, Hu H, Yuan Q, Peng G, Xia Y. Development and application of molecular-based diagnosis for 'Candidatus Liberibacter asiaticus', the causal pathogen of citrus Huanglongbing. Plant Pathol. 2006;55:630–8.
15. Trivedi P, Sagaram US, Brlansky RH, Rogers M, Stelinski LL, Oswalt C, et al. Quantification of viable Candidatus Liberibacter asiaticus in hosts using quantitative PCR with the aid of ethidium monoazide (EMA). Eur J Plant Pathol. 2009;124:553–63.
16. Almeida MR, Alves RS, Nascimbem LB, Stephani R, Poppi RJ, de Oliveira LF. Determination of amylose content in starch using Raman spectroscopy and multivariate calibration analysis. Anal Bioanal Chem. 2010;397:2693–701.
17. Zeng ZC, Hu S, Huang SC, Zhang YJ, Zhao WX, Li JF, et al. Novel electrochemical Raman spectroscopy enabled by water immersion objective. Anal Chem. 2016;88:9381–5.
18. Virkler K, Lednev IK. Blood species identification for forensic purposes using Raman spectroscopy combined with advanced analytical statistics. Anal Chem. 2009;81:7773–7.
19. López-López M, Delgado JJ, García-Ruiz C. Analysis of macroscopic gunshot residues by Raman spectroscopy to assess the weapon memory effect. Forensic Sci Int. 2013;231:1–5.
20. Cantarero A. Raman scattering applied to materials science. Procedia Mater Sci. 2015;9:113–22.
21. Kurouski D, Washington J, Ozbil M, Prabhakar R, Shekhtman A, Lednev IK. Disulfide bridges remain intact while native insulin converts into amyloid fibrils. PLoS One. 2012;7:e36989.
22. Bueno J, Lednev IK. Advanced statistical analysis and discrimination of gunshot residue implementing combined Raman and FT-IR data. Anal Methods. 2013;5:6292–6.
23. Farber C, Kurouski D. Detection and identification of plant pathogens on maize kernels with a hand-held Raman spectrometer. Anal Chem. 2018;90:3009–12.
24. Egging V, Nguyen J, Kurouski D. Detection and identification of fungal infections in intact wheat and sorghum grain using a hand-held Raman spectrometer. Anal Chem. 2018;90:8616–21.
25. Sanchez L, Farber C, Lei J, Zhu-Salzman K, Kurouski D. Noninvasive and nondestructive detection of cowpea bruchid within cowpea seeds with a hand-held Raman spectrometer. Anal Chem. 2019;91:1733–7.
26. Chiong Kelvin T, Mona B Damaj, Carmen S Padilla, Carlos A Avila, Shankar R Pant, Kranthi K Mandadi, Ninfa R Ramos, Denise V Carvalho, and T. Erik Mirkov (2017) Reproducible genomic DNA preparation from diverse crop species for molecular genetic applications. Plant methods, 13 (1), 106.
27. Rezadoost, M H, Kordrostami M, & Kumleh HH (2016). An efficient protocol for isolation of inhibitor-free nucleic acids even from recalcitrant plants. 3 Biotech, 6(1), 61.
28. Mafra V, Kubo K.S, Alves-Ferreira M, Ribeiro-Alves M, Stuart R.M, Boava L.P, Rodrigues CM, and Machado, M.A. (2012). Reference Genes for Accurate Transcript Normalization in Citrus Genotypes under Different Experimental Conditions. PLoS ONE 7, e31263.
29. Synytsya A, Čopíková J, Matějka P, Machovič V. Fourier transform Raman and infrared spectroscopy of pectins. Carb Polym. 2003;54:97–106.
30. Edwards HG, Farwell DW, Webster D. FT Raman microscopy of untreated natural plant fibres. Spectrochim Acta A Mol Biomol Spectrosc. 1997;53A:2383–92.
31. Tschirner N, Brose K, Schenderlein M, Zouni A, Schlodder E, Mroginski MA, et al. The anomaly of the ν1-resonance Raman band of bβ-carotene in solution and in photosystem I and II. Phys Stat Solid. 2009;246:2790–3.
32. Kurouski D, Van Duyne RP, Lednev IK. Exploring the structure and formation mechanism of amyloid fibrils by Raman spectroscopy: a review. Analyst. 2015;140:4967–80.
33. Agarwal UP. 1064 nm FT-Raman spectroscopy for investigations of plant cell walls and other biomass materials. Front Plant Sci. 2014;5:1–12.
34. Mary YS, Panicker CY, Varghese HT. Vibrational spectroscopic investigations of 4-nitropyrocatechol. Orient J Chem. 2012;28:937–41.
35. Yu MM, Schulze HG, Jetter R, Blades MW, Turner RF. Raman microspectroscopic analysis of triterpenoids found in plant cuticles. Appl Spectrosc. 2007;61:32–7.
36. Cao Y, Shen D, Lu Y, Huang JA. Raman-scattering study on the net orientation of biomacromolecules in the outer epidermal walls of mature wheat stems (Triticum aestivum). Ann Bot. 2006;97:1091–4.

37. Devitt G, Howard K, Mudher A, Mahajan S. Raman spectroscopy: an emerging tool in neurodegenerative disease research and diagnosis. ACS Chem Neurosci. 2018;9:404–20.
38. Adar F. Carotenoids - their resonance raman spectra and how they can be helpful in characterizing a number of biological systems. Spectroscopy. 2017;32:12–20.
39. Kang L, Wang K, Li X, Zou B. High pressure structural investigation of benzoic acid: Raman spectroscopy and x-ray diffraction. J Phys Chem C. 2016;120:14758–66.
40. Agarwal UP. Raman imaging to investigate ultrastructure and composition of plant cell walls: distribution of lignin and cellulose in black spruce wood (Picea mariana). Planta. 2006;224:1141–53.
41. Pompeu DR, Larondelle Y, Rogez H, Abbas O, Pierna JAF, Baeten V. Characterization and discrimination of phenolic compounds using Fourier transformation Raman spectroscopy and chemometric tools. Biotechnol Agron Soc Environ. 2017;22:1–16.
42. Liu Q, Luo L, Zheng L. Lignins: biosynthesis and biological functions in plants. Int J Mol Sci. 2018;19:335.
43. Bennett RN, Wallsgrove RM. Secondary metabolites in plant defence mechanisms. New Physiol. 1994;127:617–33.
44. Treutter D. Significance of flavonoids in plant resistance: a review. Environ Chem Lett. 2006;4:147–57.
45. Skadhauge B, Thomsen KK, Von Wettstein D. The role of the barley testa layer and its flavonoid content in resistance to Fusarium infections. Hereditas. 1997;126:147–60.
46. Sankaran S, Ehsani R, Etxeberria E. Mid-infrared spectroscopy for detection of Huanglongbing (greening) in citrus leaves. Talanta. 2010;83:574–581.
47. Shashilov VA, Lednev IK. Advanced statistical and numerical methods for spectroscopic characterization of protein structural evolution. Chem Rev. 2010;110:5692–713.
48. Eriksson L, Byrne T, Johansson E, Trygg J, Vikstrom C. Multi- and megavariate data analysis basic principles and applications, 3rd edn. Umetrics Academy; 2013.
49. Sankaran S, Mishra A, Maja JM, Ehsani R. Visible-near infrared spectroscopy for detection of Huanglongbing in citrus orchards. Comp Electron Agricult. 2011;77:127–34.
50. Hawkins SA, Park B, Poole GH, Gottwald T, Windham WR, Lawrence KC. Detection of citrus Huanglongbing by Fourier transform infrared-attenuated total reflection spectroscopy. Appl Spectrosc. 2010;64:100–3.
51. Vallejo-Pérez MR, Mendoza MG, Elias MG, Gonzalez FJ, Contreras HR, Servin CC. Raman spectroscopy an option for the early detection of citrus Huanglongbing. Appl Spectrosc. 2016;70:829–39.